nature energy

Article

https://doi.org/10.1038/s41560-024-01580-0

Transforming public transport depots into profitable energy hubs

Received: 12 October 2023

Accepted: 13 June 2024

Published online: 01 August 2024

Check for updates

Xiaohan Liu[1,2], Patrick Plötz[3], Sonia Yeh[4], Zhengke Liu[1], Xiaoyue Cathy Liu[5] & Xiaolei Ma[1,6]

Transportation is undergoing rapid electrification, with electric buses at the forefront of public transport, especially in China. This transition, however, could strain electricity grids. Using a large-scale dataset with over 200 million global positioning system records from 20,992 buses in Beijing, we explore the technical, economic and environmental implications of transforming public transport depots into renewable energy hubs. Here we show that solar photovoltaic reduces the grid's net charging load by 23% during electricity generation periods and lowers the net charging peak load by 8.6%. Integrating energy storage amplifies these reductions to 28% and 37.4%, respectively. Whereas unsubsidized solar photovoltaic yields profit 64% above costs, adding battery storage cuts profits to 31% despite offering grid benefits. Negative marginal abatement gains for CO_2 emissions underscore the economic sustainability. Our findings provide a model for cities worldwide to accelerate their commitments towards sustainable transport and energy systems.

To limit global temperature increase to below 1.5 °C, the transport sector faces a daunting challenge in curbing its greenhouse gas emissions, given its heavy dependence on oil[1,2]. Transportation was responsible for 26% (ref. 3) of worldwide energy consumption in 2020 and for 20% (ref. 4) of global carbon dioxide (CO_2) emissions in 2021. Road transport constituted 77% of transportation CO_2 emissions[5], of which 38% came from cars[6,7]. Public transport has emerged as a critical element in developing sustainable and equitable urban mobility infrastructures due to its low environmental impact and high passenger capacity[8]. More than half of the global population lives in cities and depends heavily on public transport services. A strategic shift from passenger cars to public transport is viewed as a key approach to reducing CO_2 emissions[9]. To combat urban air pollution and facilitate a green energy transition, China has emerged as a global leader in the deployment of battery electric buses (BEBs)[10]. Shenzhen, a bustling metropolis in China home to over 17 million residents, accomplished a notable transition from diesel and natural gas buses to BEBs in 2017 (ref. 11). This transition reduced CO_2 emissions by 1.35 million tons and an equivalent energy savings of 292 million litres of diesel in 2017 (ref. 12).

According to an International Energy Agency (IEA) net-zero road map[13] by 2050, the transport sector is anticipated to emerge as the dominant contributor to global carbon emissions, accounting for 0.7 Gt CO_2 annually. This projection underscores the notion that simply electrifying transport might not be sufficient to achieve deep decarbonization for the transport sector. Complementing this, wind and solar photovoltaic (PV) are expected to account for approximately 70% of global electricity generation[13]. However, pathways and operation models for incorporating renewable energy into the transport sector still need to be better understood. Recent studies have raised concerns regarding the potential grid impacts from large-scale transport electrification[14]. The integration of renewable energy and energy storage systems into transport electrification emerges as a potent strategy, both in further curtailing transport emissions and alleviating concerns of grid vulnerability[15–18]. Successful small-scale adoptions of solar PV and

[1]School of Transportation Science and Engineering, Beihang University, Beijing, China. [2]Department of Architecture and Civil Engineering, Chalmers University of Technology, Gothenburg, Sweden. [3]Fraunhofer Institute for Systems and Innovation Research ISI, Karlsruhe, Germany. [4]Department of Space, Earth and Environment, Chalmers University of Technology, Gothenburg, Sweden. [5]Department of Civil and Environmental Engineering, University of Utah, Salt Lake City, UT, USA. [6]Key Laboratory of Intelligent Transportation Technology and System, Ministry of Education, Beijing, China. e-mail: xiaolei@buaa.edu.cn

https://doi.org/10.1038/s41560-024-01580-0

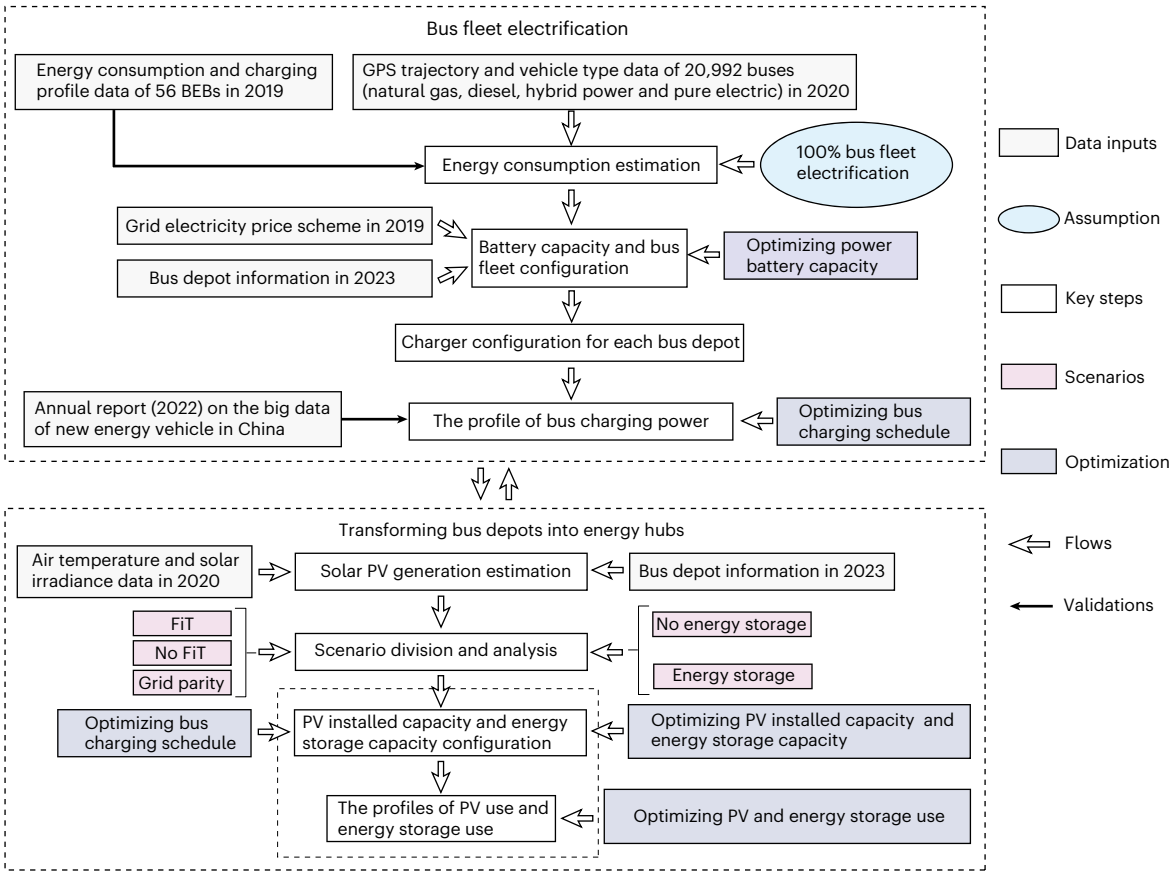

Fig. 1 | Data-driven framework for analysing comprehensive implications of transforming public transport depots into energy hubs. This framework uses Beijing's entire public transport network to illustrate how various datasets are leveraged to quantify the technical, economic and environmental benefits of transforming public transport depots into energy hubs. This framework outlines the daily BEB charging load curves at each bus depot under a 100% electrified bus system scenario. The framework maximizes the economic profits of solar PV and energy storage by optimizing the PV installed capacity, energy storage capacity, bus charging schedules, solar PV use and energy storage use. The framework can simulate daily BEB charging schedules, solar PV usage and energy storage usage, offering minute-by-minute resolution and accounting for seasonal variations. Here FiT denotes the feed-in-tariff policy.

energy storage systems with electric vehicle (EV) charging have been piloted across many cities in China, including Shanghai, Quanzhou, Hangzhou, Xian and Chongqing[19–23]. In these instances, solar PV energy for EV charging typically relies on a microgrid involving charging infrastructures, rooftop PV panels, energy storage systems, microgrid controllers and metering and communication infrastructure[24].

Integrating onsite solar PV and energy storage (PES) at bus depots introduces a renewable energy production and management mode, transforming a public transport depot into a future energy hub. A few pioneering studies have established mathematical models for the integration of public transport, renewable energy, intelligent microgrids, public grids, and pricing mechanisms[25,26]. In addition, several studies have investigated the planning and operating problems of the integration of solar PV, energy storage, and public transport systems[27–30]. Existing studies have yet to understand the economic, environmental and grid-related implications of integrating public transport, solar PV and energy storage on a citywide scale using extensive real-world data. There is a pressing need for a universal framework that melds data and model-driven approaches to unlock insights for the widespread adoption of solar PV and energy storage within urban public transport networks.

The present study goes beyond existing studies in several ways. First, we use city-scale empirical data of BEB trajectories. Second, we provide a comprehensive impact analysis of the integration of solar PV and energy storage into a fully electrified bus system. Third, we develop a holistic optimization framework combining solar PV, energy storage, time-of-use electricity pricing and bus charging schedules. This work first simulates a baseline scenario in which BEBs replace all buses of other fuel types in Beijing. The complete bus fleet electrification is simulated based on a rich dataset of bus global positioning system (GPS) trajectory data, vehicle type data, grid electricity price schemes and bus depot data. These four real-world datasets are used to simulate BEB energy consumption, optimize BEB battery capacities and optimize BEB charging schedules under perfect foresight. To transform bus depots into energy hubs, this framework estimates solar PV generation based on bus depot data, air temperature data and solar irradiance data. Combined with three scenarios related to subsidy policies for solar PV, we maximize the economic profits for solar PV and energy storage by optimizing the installed capacity of solar PV, energy storage capacity, bus charging schedules, solar PV use and energy storage use.

Our study explores the impacts and economic feasibility of integrating electric public transport systems with rooftop solar PV and energy storage systems at bus depots in Beijing, exploring economic trade-offs, effects on the grid and environmental advantages. The results reveal that converting bus depots into profitable energy hubs generates economic gains and CO_2 savings. Furthermore, the net grid charging load of BEBs can be alleviated.

Simulating the largest electric bus fleet

By 2021, low- or no-emission buses constituted 91.06% of Beijing's fleet[31]. As the world's largest public transport system, Beijing public transport system boasted 1,640 bus routes with a total route length

of 42,860 km, supported by 27,731 buses and housed across 709 bus depots by 2022 (ref. 32). Most chargers in Beijing public transport system had a maximum charging power of 450 kW by 2022 (ref. 33).

Figure 1 illustrates a data-driven framework for analysing comprehensive implications of transforming public transport depots into energy hubs. As shown in Fig. 1, we collect two datasets: bus GPS trajectory data and vehicle information from 2020 in which BEBs constituted approximately 40% of the entire bus fleet. From these two datasets, we retrieve 20,992 buses, 1,141 bus lines and 678 bus depots in Beijing. We use bus GPS trajectory records to determine the timing and duration of buses' layovers at bus depots. We employ an opportunity charging strategy where BEBs are charged during layovers at bus depots whenever the chargers are available. We define a baseline scenario of 100% BEBs simulated by successively estimating BEB energy consumption, optimizing BEB battery capacities and optimizing BEB charging schedules. To optimize BEB charging schedules, we establish a mixed integer linear programming model to determine charging power and time for each BEB aligning with the opportunity charging strategy. The simulation results provide detailed spatial–temporal profiles of BEB charging needs with minute-by-minute resolution.

Details related to the BEB infrastructure in 2020 and the baseline scenario are presented in Table 1. The simulation results indicate that the baseline scenario requires 2,972 chargers across 678 bus depots. The vehicle-to-charger ratio increases from 6.6 to 8.1. Our analysis estimates that the lifetime battery requirement for 24,031 BEBs stands at 26,071 BEB batteries, averaging about 1.1 batteries per BEB over its lifespan (13 years).

Figure 2 shows bus fleet electrification results under the baseline scenario. Specifically, Fig. 2a shows the distribution of chargers required at various bus depots. Notably, 75% of bus depots are equipped with five or fewer chargers. The mean and medium numbers of chargers deployed at a bus depot are 4.4 and 3.0, respectively. This observation is consistent with the observed daily charging demands at bus depots, further illustrated in Supplementary Fig. 1. Figure 2b displays the optimal BEB battery capacities, with an average value of 221 kWh. Supplementary Fig. 2 presents the estimated energy consumption of BEBs in April and December separately, with an average consumption of 159 kWh in December. Figure 2c highlights the daily BEB charging load profiles. We illustrate the average, minimum and maximum BEB charging loads throughout the year, broken down by each minute of the day. Our optimization model for BEB charging avoids the overlap of charging load peaks and the peak electricity price period (18:00–21:00 in Beijing). Surges in BEB charging typically occur at the transition points between different electricity price periods and the date transition point at 0:00. Supplementary Fig. 3 shows that most BEBs are parked at bus depots between 0:00 and 5:00. This pattern accounts for the concentration of BEB charging demands mainly between 0:00 to 5:00. In addition, the seasonal variations in BEB charging loads are distinctly observable due to the seasonal fluctuations in BEB energy consumption. Figure 2d shows the minimum and maximum city loads in Beijing in 2019 (including simulated BEB charging loads) detailed on a minute-by-minute basis throughout the year. Figure 2e shows the minimum and maximum proportions of BEB charging load on city load in Beijing in 2019 minute-by-minute over a year. The proportions range from 0% to 4% and show a similar daily profile with BEB charging loads. The seasonal impacts on the ratio of peak BEB charging load to the city load are shown in Fig. 2f, which illustrates the ratio of peak BEB charging load to the city load at the time point (0:00) in different months, fluctuating between 2.4% and 3.9%. We also show the proportions of BEB charging loads on city loads in March and June in Fig. 2f.

The weekday load, excluding the BEB charging load in Beijing (Supplementary Fig. 4), exhibits a peak period from 11:00 to 12:00, and the peak time is not shifted when the BEB charging load is considered. Supplementary Table 1 presents the peak load periods and peak loads of different months in Beijing. A comparison of our simulation results with real BEB operational data in China, illustrated in Supplementary Fig. 5, demonstrates consistency regarding charging event distribution and energy consumption.

Table 1 | Electric bus infrastructure in 2020 and the simulated baseline scenario

Year	2020	Baseline scenario
Number of BEBs	8,397	24,031
Number of buses with other fuels	12,595	0
Number of chargers	1,278	2,972
Bus depots with charging infrastructure	216	678
Vehicle-to-charger ratio	6.6	8.1

We also investigate the impacts of the maximum charging power per charger on the bus fleet electrification and charging infrastructure deployment. Supplementary Table 6 presents the sensitivity analysis results of the maximum charging power per charger. The total investment in electric buses, chargers and power batteries initially rises and then falls as the maximum charging power increases from 100 kW to 600 kW per charger. This trend is accompanied by a decrease in the number of BEBs and chargers required, underscoring the importance of strategic charger capacity planning by public transport authorities in extending bus charging networks.

Transforming public transport depots into energy hubs

An energy hub can be generally defined as an integrated framework in which various energy sources are converted, stored and optimized[34,35]. To transform public transport depots into energy hubs, we leverage the air temperature, solar irradiance and building rooftop surface area at bus depots to simulate the hourly solar PV output power at each bus depot throughout 2020 in Beijing. We design an electric public transport network that integrates onsite rooftop solar PV and energy storage at bus depots, as illustrated in Fig. 3. The energy flows at each energy hub include solar PV energy use for charging BEBs, solar PV energy sales to the grid, solar PV energy use for charging energy storage, grid electricity purchase for charging energy storage, energy storage use for charging BEBs and grid electricity purchase for charging BEBs.

In the past decade or so, the levelized cost of electricity (LCOE) of solar PV was higher than the local benchmark price set for desulfurized coal plants[36]. Therefore, the Chinese government promoted solar PV adoption by implementing a feed-in-tariff (FiT) policy. However, with the declining LCOE of solar PV, the corresponding subsidy has been gradually reduced[37,38]. To understand the economic benefits of energy hubs, we introduce three market scenarios concerning the price of unused PV electricity and solar PV costs. FiT denotes the market scenario where utilities buy unused PV electricity at a government-regulated price higher than the LCOE of solar PV and the local benchmark grid electricity price of local desulfurized coal plants (US$0.057 kWh^{-1}). No FiT denotes the market scenario where utilities buy unused PV electricity at the local benchmark grid electricity price of local desulfurized coal plants (US$0.051 kWh^{-1}). Grid parity denotes the market scenario where the solar PV cost is reduced to US$589 kW^{-1} (from US$629 kW^{-1}) such that the LCOE of solar PV matches the local benchmark grid electricity price of local desulfurized coal plants and where utilities buy unused PV electricity at the local benchmark grid electricity price of local desulfurized coal plants (US$0.051 kWh^{-1}).

The key economic assumptions for each market scenario are also listed in Table 2. We present daily operational solutions to maximize the economic benefits of solar PV and energy storage by solving mixed integer linear programming models (Methods). The proposed mixed integer linear programming models capture the dynamics of energy flows at energy hubs with minute-by-minute resolution.

https://doi.org/10.1038/s41560-024-01580-0

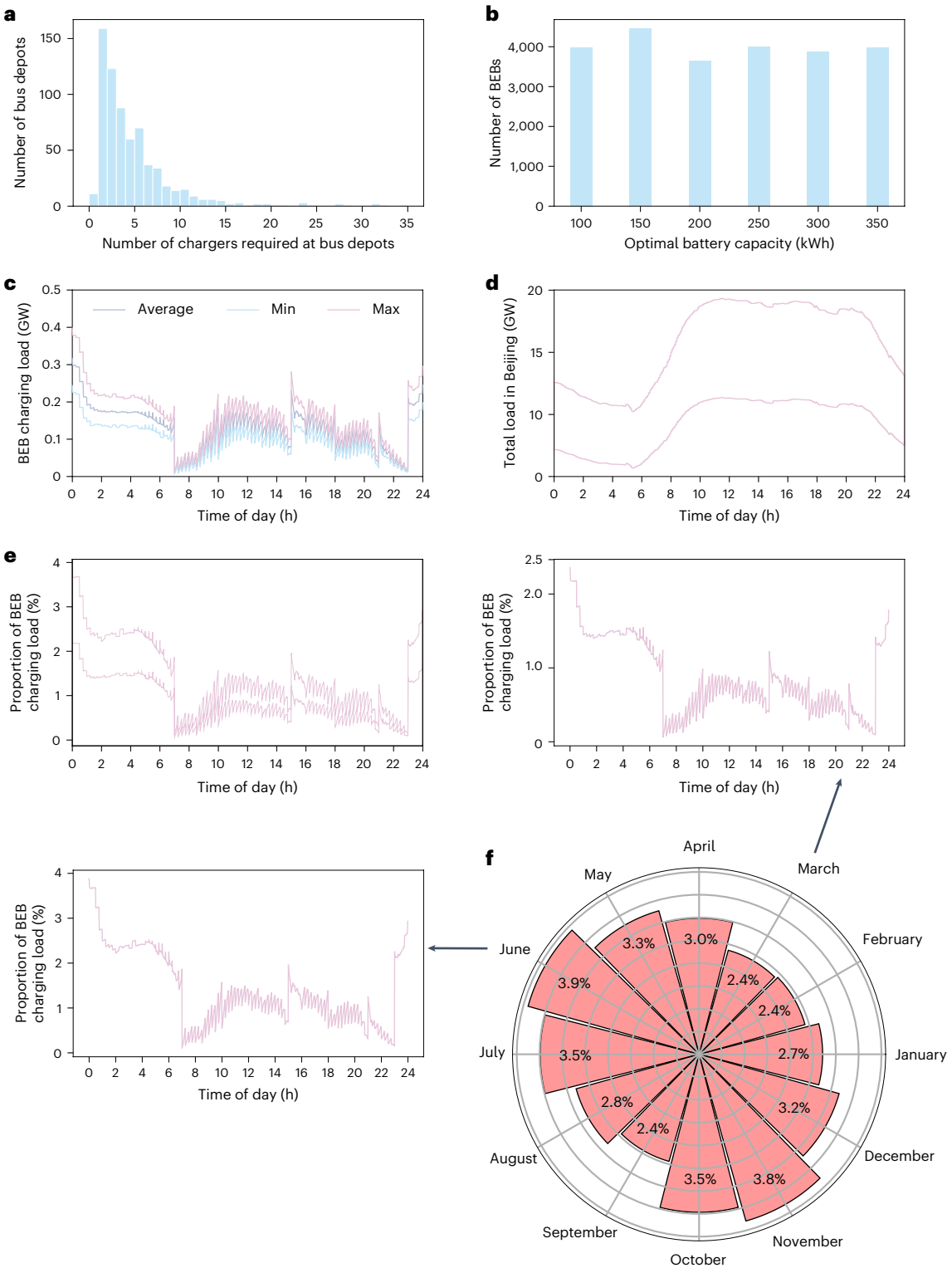

Fig. 2 | Bus fleet electrification results in the baseline scenario. a, The number of chargers required at bus depots with a mean of 4.4. **b**, The optimal battery capacity for battery electric buses (BEBs) with a mean of 221 kWh. **c**, The average, minimum and maximum BEB charging loads within a day across the span of a year. **d**, The minimum and maximum city loads in Beijing in 2019 (including BEB charging loads) within a day across the span of a year. **e**, The minimum and maximum proportions of BEB charging load on city load in Beijing in 2019 within a day across the span of a year. **f**, The ratio of peak BEB charging load to the city load at the time point (0:00) in different months. The daily profiles of BEB charging load on city load in March and June are highlighted in **f**.

Seasonal solar PV variability impact on grid loads

The utilization pattern of solar PV and energy storage is shaped by factors such as the BEB charging schedule, grid electricity prices, solar PV electricity sales prices and seasonal variations. Furthermore, charging BEBs introduces additional loads to the grid, whereas PV reduces this load by producing electricity. To understand these impacts, we illustrate solar PV yields, usage and net-load impacts on the grid under each market scenario in Fig. 4.

https://doi.org/10.1038/s41560-024-01580-0

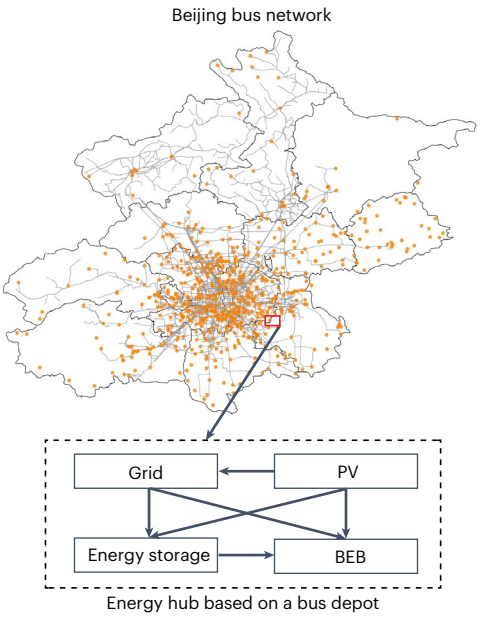

Fig. 3 | Electric public transport network integrated with rooftop solar PV and energy storage. Battery electric buses (BEBs) are charged at bus depots with chargers, and the electricity demand is supplied by the grid, solar PV and energy storage. The orange dots represent bus depots, and the red rectangle indicates the selected bus depot to be transformed into an energy hub.

The monthly solar PV yield and usage under the FiT, no FiT and grid parity scenarios are shown in Fig. 4a–c, respectively. The rate of solar PV self-consumption fluctuates between 42% and 60% without energy storage in different months. With energy storage, this self-consumption rate spans from 43% to 65%. The highest and lowest rates of self-consumption of solar PV energy occur in July and April, respectively. The maximum solar PV production is in April, whereas the minimum occurs in November. Notably, the solar production in the no FiT scenario (Fig. 4b) is only 0.08% lower than those in the FiT and grid parity scenarios (Fig. 4a,c). This result implies that utilizing almost all the available rooftop areas for PV panel installations at bus depots remains an optimal decision, even without economic incentives. We find that the rate of solar PV self-consumption under the FiT scenario is less than that in the no FiT and grid parity scenarios due to the economic benefits of selling solar PV electricity.

Figure 4d,e illustrates the net daily grid loads from BEB charging for April and July of the year under the grid parity scenario with baseline, PV and PES. The net daily grid loads from BEB charging of other months are shown in Supplementary Fig. 6. The grey purple lines depict the original daily grid loads from BEB charging without PV and PES. The blue and pink lines represent the altered net daily grid loads of BEB charging with the introduction of PV and PES, respectively. In the daytime, the net daily grid loads of BEB charging with PV and PES show an average reduction of 23% and 28%, respectively, compared with the baseline net daily grid loads of BEB charging across different months. The most substantial decline is noted in April, with an average decrease of 31% and 37% with PV and PES, respectively. Conversely, the most minor reduction occurs in July, showing an average 19% and 24% reduction with PV and PES, respectively. The seasonal fluctuation ranges within 9% of the reduction in net daily grid loads from BEB charging. This result highlights seasonal solar PV variability impact on grid loads. The peak net daily grid loads (at 0:00) of BEB charging are reduced by 7% to 10% and 36% to 39% across different months with PV and PES, respectively. Supplementary Fig. 7 shows the net daily grid loads from BEB charging under the FiT and no FiT scenarios with PV and PES. The orange lines depict the average daily grid loads over a year from BEB charging without PV and PES. The green and red lines capture the average net daily grid loads of BEB charging over a year with the introduction of PV and PES, respectively. Under the no FiT scenario, the net daily grid loads of BEB charging with PV and PES show an average reduction of 23% and 28% compared with the original net daily grid loads of BEB charging, aligning with the results observed in the grid parity scenario. The peak net daily grid loads of BEB charging are reduced by 8.6% and 37.4% with PV and PES, respectively. Under the FiT scenario, the positive impact on net grid loads is slightly less than the results seen in both the no FiT and grid parity scenarios.

We show the reduced net daily grid loads from BEB charging under the FiT, no FiT and grid parity scenarios for different energy hubs during daytime in Supplementary Fig. 8. For each energy hub, we calculate the average reduction in the net daily grid loads of BEB charging over various months. For the no FiT and grid parity scenarios, the mean reduction stands uniformly at 78 kW with PV. Incorporating energy storage further elevates this reduction to 110 kW for each scenario. Consistently, the standard deviation of the decrease with PV is 81 kW for each scenario. With PES, the standard deviation increases slightly to 92 kW for each scenario. For the FiT scenario, the mean reduction is slightly less than that for the no FiT and grid parity scenarios. These findings highlight the substantial and variable impacts of solar PV on reducing the net daily grid loads of BEB charging across different energy hubs.

Table 2 | The key economic assumptions for each market scenario

Economic assumptions	FiT	No FiT	Grid parity
Solar PV cost (US$ kW^{-1})	629	629	589
LCOE of solar PV (US$ kWh^{-1})	0.054	0.054	0.051
Electricity price of solar PV sales (US$ kWh^{-1})	0.057	0.051	0.051
Energy storage cost (US$ kWh^{-1})	223	223	223

Economic advantage of public transport energy hubs

Figure 5 shows the economic analysis of solar PV and energy storage overall and at each energy hub throughout their lifetime of 25 years. The net present value results reflecting the costs and benefits of solar PV and energy storage across varying scenarios are depicted in Fig. 5a–c. Notably, the three scenarios find a net profit of 64% to 76% of the solar PV cost without energy storage. However, when solar PV is integrated with energy storage, the net profit shrinks to 31% to 37% of the combined cost of PES. In Fig. 5a–c, the grid electricity purchase cost of energy storage refers to the expense incurred from purchasing grid electricity at a relatively low price to be stored in the energy storage system.

We define profitability as the ratio of the net profit to the cost associated with solar PV and energy storage. The profit is derived from feed-in revenue and savings in BEB charging costs. Figure 5d–f illustrates the profitability of solar PV and energy storage at each energy hub throughout its lifetime. The profitability with PV almost ranges from 0% to 150%, with over half of the energy hubs achieving profitability greater than 100%. Figure 5g–i shows the net profit of solar PV and energy storage at each energy hub throughout its lifetime. The variability of profitability and net profit highlights the differing economic solar PV impacts across distinct energy hubs. The main reason for these varying impacts is the considerable differences in charging demand distribution and solar PV generation across energy hubs. As Supplementary Fig. 9 shows, such differences further lead to the various levels of the mismatch between charging needs and solar PV generation. After introducing energy storage, 17% to 22% of energy hubs exhibit negative net profits, suggesting that the sum of feed-in revenue and charging cost savings does not offset the cost of PES, given the prevailing investment prices for energy storage.

https://doi.org/10.1038/s41560-024-01580-0

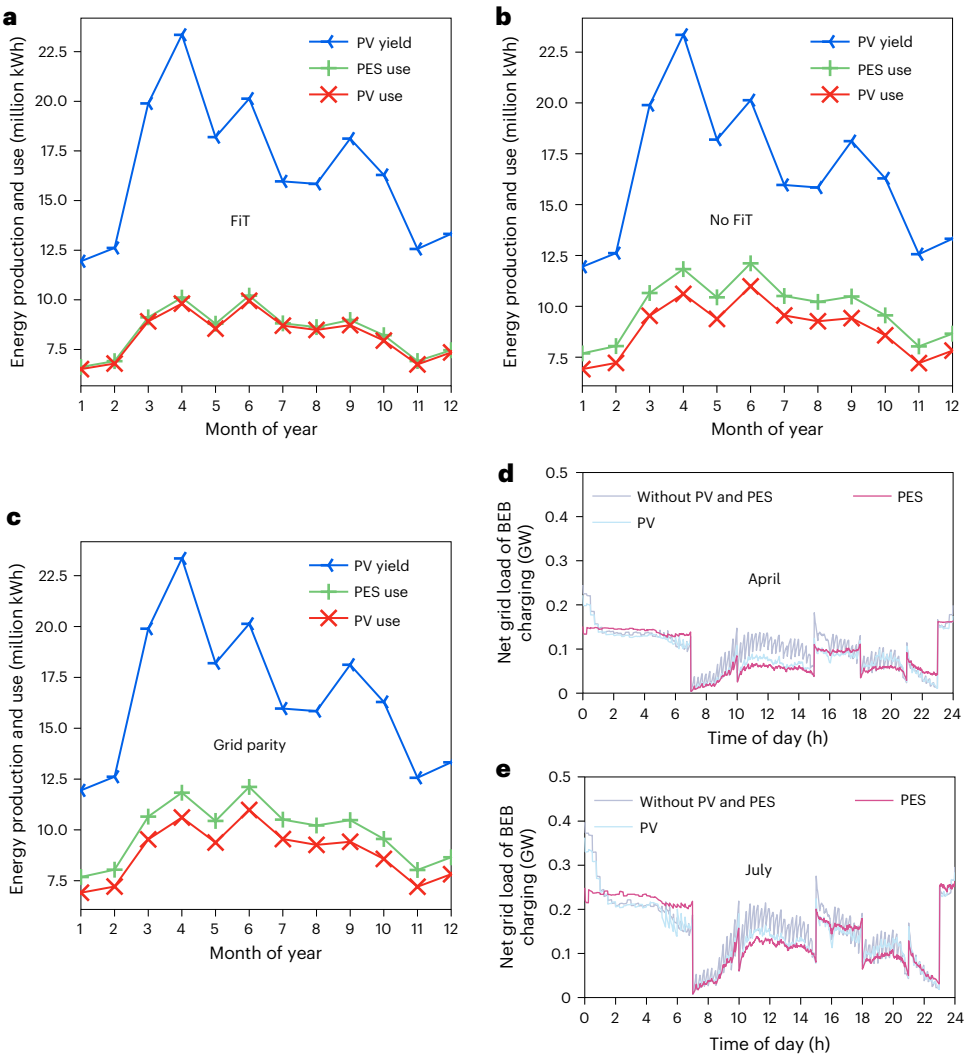

Fig. 4 | Net-load impacts on the grid under each market scenario at energy hubs. a–**c**, Monthly solar PV yield and usage under the FiT (**a**), no FiT (**b**) and grid parity (**c**) scenarios. **d**,**e**, The net daily grid loads from battery electric bus charging for April (**d**) and July (**e**) of the year under the grid parity scenario with baseline (grey purple), PV (blue) and solar PV and PES (pink). The net grid load of BEB charging reflects the actual load supported by the grid, excluding the portion of the load supplied by the energy hubs.

We also examine the impact of energy storage cost, energy storage resale price and grid electricity price on the net profit of solar PV and energy storage. Taking the grid parity scenario as an example, we perform a sensitivity analysis on these three parameters. Supplementary Fig. 10 shows the sensitivity analysis results of energy storage cost on the net profit of solar PV and energy storage at each energy hub throughout its lifetime. Notably, when the energy storage cost drops to 70% (US$156 kWh^{-1}) of the current cost (US$223 kWh^{-1}), the median of the net profit of PV and PES approaches parity. Supplementary Fig. 11 illustrates how the energy storage resale price influences the net profit of solar PV and energy storage at each energy hub throughout its lifetime. The findings reveal that the energy storage resale price exerts minimal influence on the net profit of PES. Supplementary Fig. 12 presents the sensitivity analysis results of grid electricity pricing on the net profit of solar PV and energy storage at each energy hub throughout its lifetime. The results show an apparent increase in the net profit of PES as the gap between peak and off-peak grid electricity prices widens. Notably, the median of the net profit of PES surpasses that of PV when the price differential reaches US$0.115 kWh^{-1}. This sensitivity analysis demonstrates the impact of energy storage cost and grid electricity pricing on the net profit of integrating solar PV with energy storage at bus depots. As energy storage technology continues to evolve, the economic benefits of PES are expected to increase with reductions in energy storage costs. Additionally, this analysis indicates that the economic advantages of combining solar PV with energy storage are stronger in scenarios with a substantial difference between peak and off-peak grid electricity prices.

Economics of carbon savings in a sustainable world

We calculate the CO_2 emissions associated with BEBs and energy hubs in the operational phase. To be conservative in terms of CO_2 savings, we select the reference case of the projected electricity production and CO_2 emissions tailored to the net-zero emissions by 2050 scenario[13]. According to China's grid carbon emissions factor in 2021, we derive China's future carbon emissions factors to align with the net-zero scenario. Table 3 presents the total calculated CO_2 emissions across various scenarios from 2021 to 2045. We count the carbon emissions associated with solar PV production and energy storage operation. The overall carbon emissions reductions from integrating solar PV range from 1.4% to 5.7% relative to the baseline scenario. Integrating energy storage does not further decrease emissions under the no FiT and grid parity scenarios due to the associated emissions of energy storage and grid electricity purchased for energy storage. In contrast, under the FiT scenario, integrating energy storage reduces the amount of solar

https://doi.org/10.1038/s41560-024-01580-0

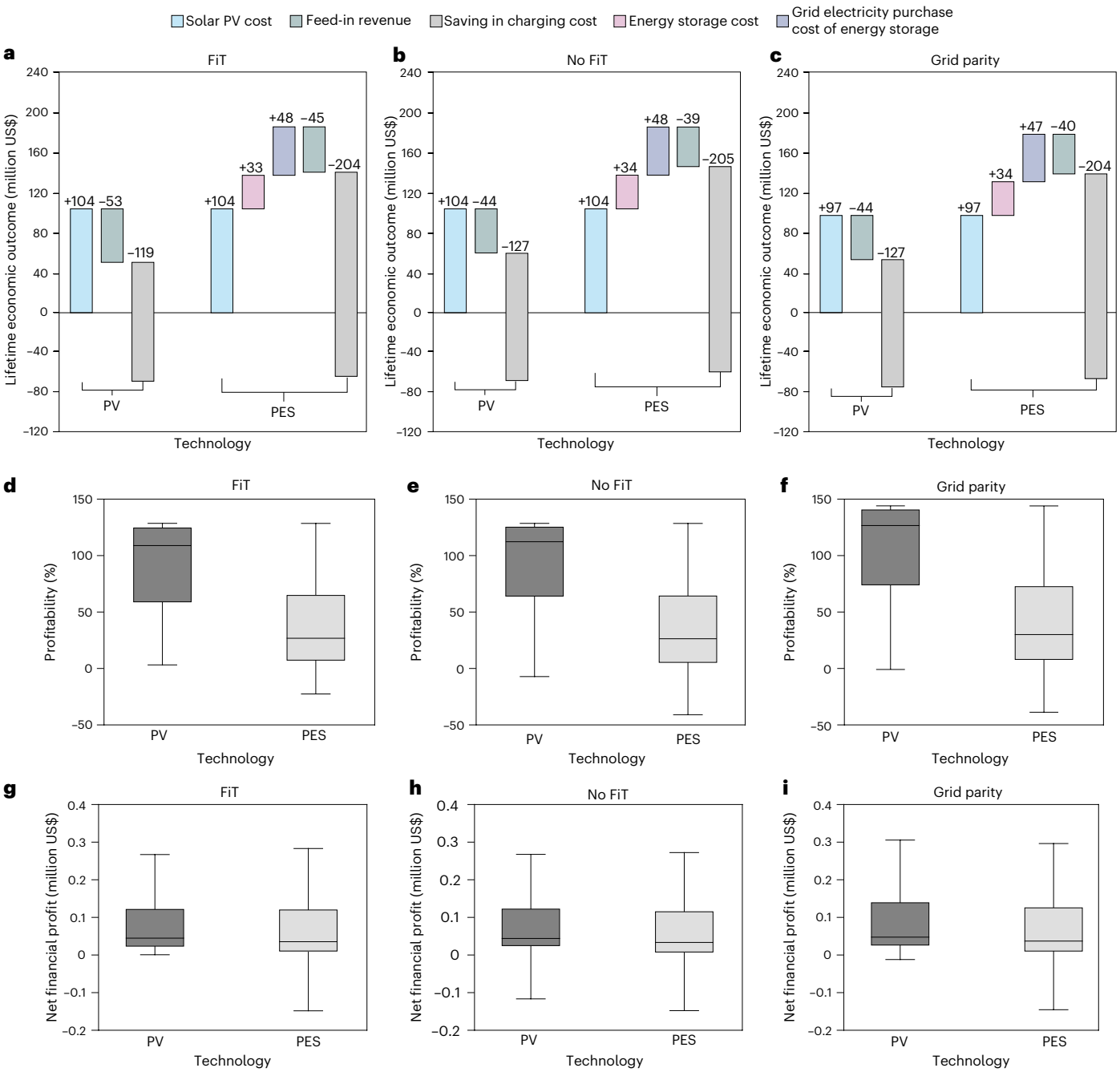

Fig. 5 | Economic analysis of solar PV and energy storage. a–c, The figure illustrates the lifetime economic outcomes for solar PV and PES overall and across 678 energy hubs under three scenarios: the total lifetime costs and benefits with the FiT (**a**), no FiT (**b**) and grid parity (**c**) scenarios, respectively. **d–f**, The profitability of these systems across 678 energy hubs under the FiT (**d**), no FiT (**e**) and grid parity (**f**) scenarios. **g–i**, The net profit of solar PV and energy storage across 678 energy hubs, also under the FiT (**g**), no FiT (**h**) and grid parity (**i**) scenarios. In **d–i**, the top and bottom of the box are the 75th and 25th percentiles, and the median is represented by the horizontal line internal to the box. The boundary of the lower whisker is the minimum value, and the boundary of the upper whisker is the maximum value after excluding outliers.

PV electricity sold back to the grid, thereby increasing CO_2 emissions savings. The results also indicate that the CO_2 emissions reduction under the FiT scenario is lower than those under the no FiT and grid parity scenarios. This discrepancy is primarily attributed to economic incentives under the FiT scenario, which reduces the utilization of solar PV energy compared with scenarios lacking such subsidies.

It is critical to consider the potential of negative marginal abatement costs (that is, profitable projects) associated with local renewable energy initiatives and the transition of the energy sector towards economic sustainability. The marginal abatement cost of solar PV falls between −US$259 t^{-1} CO_2 and −US$223 t^{-1} CO_2, whereas the marginal abatement costs of solar PV and energy storage fall between −US$220 t^{-1} CO_2 to −US$193 t^{-1} CO_2 and are slightly less profitable. The negative marginal abatement costs indicate that both PV and PES options are profitable investments for reducing carbon emissions across each market scenario. The carbon emissions factors of regional grids influence the effects of carbon emissions reduction. Obviously, as the proportion of green electricity generation increases for power plants, the CO_2 emissions reduction attributable to solar PV and energy storage diminishes. Nonetheless, understanding the

Table 3 | Total CO_2 emissions (in 1,000 tonnes) under each market scenario from 2021 to 2045

Scenario	Solar PV	Energy storage	Grid electricity for storage	Grid electricity for charging BEBs directly	Total
Baseline	NA	NA	NA	5,277	5,277
FiT—PV	191	NA	NA	4,823	5,014
FiT—PES	191	7	298	4,491	4,987
No FiT—PV	191	NA	NA	4,786	4,977
No FiT—PES	191	7	295	4,484	4,977
Grid parity—PV	191	NA	NA	4,786	4,977
Grid parity—PES	191	7	292	4,487	4,977

NA, not applicable.

marginal abatement costs is essential when comparing the advantages of different pathways for CO_2 emissions reductions.

Discussion

In this study, we examine the innovative integration of energy storage and solar PV systems within bus depots, demonstrating a viable strategy for uniting the renewable energy and public transport sectors. We demonstrate a case of transforming public transport depots into profitable future energy hubs. Our findings provide evidence that the transition from a consumer to a prosumer for bus depots can alleviate pressure on the grid and have broader implications for grid reliability and resilience. With the revised Clean Vehicles Directive presenting Europe's minimum quotas for low- and zero-emission buses[39], similar implications of bus fleet electrification could arise for the grids. This study provides a pathway for other countries to mitigate grid vulnerability and consider investment returns by transforming bus depots into energy hubs. Furthermore, our findings could catalyse policy measures to expedite the deployment of solar PV and energy storage at other large-scale energy consumption centres, such as public EV charging stations and railway stations.

The economic analysis offers a nuanced understanding of how market dynamics could shape the uptake of this innovative model. Under various electricity pricing policies and solar cost scenarios—FiT, no FiT and grid parity, our results demonstrate promising economic benefits of investing in solar PV with or without battery energy storage. Compared to only using solar PV, introducing energy storage could increase net profits when the difference between peak and off-peak grid electricity prices increases or energy storage costs decline. Multiple levels of mismatch between charging needs and solar PV generation lead to considerable variations in profitability across energy hubs. The high mismatch between charging needs and solar PV generation could lead to low solar PV utilization, resulting in low charging cost savings. To mitigate the high mismatch, one of the potential solutions is to optimize bus routes and vehicle schedules to align with travel demands and solar PV generation at the spatio–temporal dimension. Besides, exploring various business modes and a greater range of energy storage services could further enhance net profits for energy hubs. Integrating business modes of energy storage services requires deep considerations of sustainable economic ecosystems, different stakeholders, social equity and environmental impacts. Our proposed framework lays the foundational analysis and offers a basis for future expansions by integrating additional mathematical models and analytical tools to assess the potential of solar PV and energy storage comprehensively.

Another contribution of this work lies in its implications for carbon emissions reductions. The integration of solar PV and energy storage can lead to additional emissions reductions of up to 5.7% compared with a green baseline emissions scenario. The combined advantages of economic profitability and emissions mitigation present a persuasive case for a sustainable strategy that bridges the renewable energy and public transport sectors. There is a fact that the reduction of carbon emissions from solar PV and energy storage will decrease as the electricity industry shifts towards greener sources. Nevertheless, when assessing the economic value of carbon savings, it is critical to consider the marginal abatement costs associated with local renewable energy initiatives and the transition of the energy sector towards sustainability.

In summary, our research outlines a strategically viable and economically sustainable model for incorporating solar PV and energy storage systems into existing infrastructure. We present a data-driven framework capable of simulating a fully electrified bus system scenario, optimizing energy hub operations and optimizing bus charging schedules with minute-by-minute resolution at a city scale. Results from a case study in Beijing demonstrate that transforming public transport depots into profitable energy hubs yields economic benefits, CO_2 emissions reductions and net grid load reductions. This study propels our understanding of the synergistic benefits of combining these technologies and provides actionable insights for policymakers, urban planners and the renewable energy community at large. By demonstrating such a model's viability and economic advantages, policymakers may be encouraged to prioritize similar renewable energy strategies, possibly accompanied by incentive mechanisms, to fast track urban decarbonization efforts. However, several factors, such as historical climate data, evolving government policies and potential technological advancements, constrain the proposed framework. Future work should explore the long-term operational durability of the integrated systems and consider external factors such as energy market dynamics and advancements in energy storage technologies.

Methods

Datasets

We utilize the two-part tariff of the electricity price scheme for sizeable industrial electricity consumption in Beijing[40]. We collect bus GPS trajectory data from Beijing, China, which comprise over 200 million activity records from 20,992 buses on a single day—19 October 2020. These activity records, sampled at several-second intervals, contain critical information such as unique bus IDs, timestamps, coordinates and speed. Additional bus details, such as vehicle size, weight and fuel type, are compiled in the vehicle type dataset. The unique bus ID is a conjoint field between the GPS trajectory databases and vehicle type tables. The China Meteorological Administration provides datasets comprising hourly air temperature, direct normal irradiance and diffuse horizontal irradiance of 366 days in 2020 from a national basic meteorological station in Beijing. We further retrieve the geolocation of bus depots from the Gaode Satellite Map, and 678 bus depots are identified. To estimate the solar PV potential of these bus depots, we utilize the online measurement tools available on the Gaode Satellite Map platform. During this process, we eliminate the area occupied by roof obstacles. The energy consumption profile dataset containing more than 210,000 records of 56 BEBs in 2019 in Beijing was collected by ref. 41. Uniformity is maintained in the vehicle size (12,000 mm × 2,540 mm × 3,040 mm), vehicle weight (13,000 kg) and bus battery type (lithium-titanite battery). Each record provides the start time, end time of a trip, location coordinates and energy consumption. This dataset is used to validate the energy consumption estimation method used in this study. Furthermore, we assess our BEB charging simulation results by comparing the national average charging demand distribution in China for 2022 (ref. 42).

Energy consumption estimation

The 20,992 buses used in this study feature various vehicle sizes, weights and fuel types (natural gas, diesel, hybrid power and pure electric). The energy consumption estimation assumes replacing buses of other fuel types with BEBs. Notably, the original sizes and weights of these buses are retained to facilitate characterizations of different potential BEB sizes under the baseline scenario.

The BEB energy consumption is estimated utilizing the longitudinal dynamics model[43] described in Supplementary Note 1. This model formulates energy consumption through an integral operation. We approximate the integral equation by the synthetic driving profiles generated via GPS trajectory data. Generating synthetic driving profiles aims to fit the vehicle velocity curves with GPS trajectory data. Three types of velocity curve are defined for the two adjacent GPS points: uniform speed, acceleration and deceleration. When the vehicle velocities of two adjacent GPS points are not zero, the uniform motion is approximated using the average of velocities of two adjacent GPS points. The vehicle is regarded as acceleration or deceleration when one of the two velocities equals zero. It signifies that the vehicle is stationary when both velocities are zero. Subsequently, the longitudinal dynamics model is used to estimate the energy consumption for the trip segment between two adjacent GPS points. The accumulation of all trip segments can obtain trip energy consumption. Moreover, we learn the seasonal variations in BEB energy consumption from the reference dataset[41]. Then we refine our estimations of BEB energy consumption to reflect these seasonal variations. Specifically, we define BEB energy consumption in April in Beijing as a baseline by considering the average air temperature. Subsequently, we calculate the ratios of monthly BEB energy consumption relative to April using the reference dataset[41]. Finally, we adjust our monthly energy consumption estimation according to the calculated ratios. The details of the parameter settings for BEB energy consumption are provided in Supplementary Table 3.

Optimization of BEB battery capacity

Given the estimated energy consumption at the trajectory level, we proceed to make three decisions for each natural gas, diesel or hybrid power bus in our dataset to accomplish a fully electrified bus fleet. The first decision determines the number of BEBs required to replace an existing bus of other fuel types. The second decision involves finding an optimal battery energy capacity for each bus. The last decision determines the amount of charged electricity during each bus layover. We aim to find the optimal solutions to the three decisions simultaneously. According to our brief survey of the BEB market in China[44], we set six potential battery capacities for equipping into BEBs: 100 kWh, 150 kWh, 200 kWh, 250 kWh, 300 kWh and 350 kWh. The current service trips of an existing bus of other fuel types should be fulfilled without departure delays when BEBs replace the bus. The state of charge (SoC) of BEBs should be maintained between 20% and 100%, and BEBs can only be charged during layover periods at bus depots. For a natural gas, diesel or hybrid power bus, we initially set the number of BEBs required to be one, and we determine the amount of charged electricity successively as the battery capacity increases from 100 kWh to 350 kWh. If a single BEB, even with a battery capacity of 350 kWh, cannot fulfil all service trips by meeting the SoC and charging time constraints, the number of BEBs required is increased by one. This process is repeated until all service trips are satisfied.

To simulate BEB charging, we apply the opportunity charging strategy to charge BEBs. When the chargers are available, BEBs at bus depots are charged until the layover time exhausts or the SoC reaches 100%. We utilize an empirical capacity ageing model[45] to calculate the remaining BEB battery capacity year by year. Notably, the power batteries should be retired once the remaining battery diminishes below 80% of its initial energy capacity[46]. Detailed computations involving battery fading are provided in Supplementary Note 2. We choose the optimal battery capacity for each replaced BEB to minimize the total battery purchase cost of the BEB lifetime. The other parameter settings are presented in Supplementary Table 2.

Determining charger deployments

According to the amount of charged electricity during each bus layover, we can determine the number of chargers required at bus depots. The amount of charged electricity changes as the BEB battery capacity fades during its lifetime. Hence, it is necessary to define a reference scenario for charger deployments. We establish the reference scenario where we randomly sample the residual battery capacity for each BEB from 80% to 100% of the initial capacity. Next, we arrange all charging events in chronological order for each bus depot based on the arrival times of the BEBs. We initially set the number of chargers required at each bus depot to one. As we traverse all ordered charging events, we locate a start time for each charging event within the available layover time, ensuring that each charging event is assigned a specific start time. Whenever there are no unoccupied time slots for chargers charging BEBs, the required number of chargers is increased by one. This process is repeated until every charging event is allocated a charging timetable. Notably, there is a case where multiple BEBs replace a single natural gas, diesel or hybrid power bus. In this case, we provide a bundled timetable for these BEBs as a group instead of allocating a specific timetable to each BEB, avoiding the enumeration of the combinations of charging timetables for BEBs.

Optimizing bus charging schedules

We optimize bus charging schedules at minute-by-minute resolution by solving a mixed integer programming model to minimize bus charging costs. For a bus depot in a month, the mixed integer programming model is introduced as follows.

$$\min \lambda_{\text{peak}} p_{\text{peak}} + \sum_{k\in K}\sum_{j\in J} \lambda_j q_{kj}, \tag{1}$$

$$x_{kj} \le \delta_{kj}, \forall k \in K, j \in J, \tag{2}$$

$$\sum_{j\in J} q_{kj} = Q_k, \forall k \in K, \tag{3}$$

$$q_{kj} = \Delta t_{kj} p_{kj}, \forall k \in K, j \in J, \tag{4}$$

$$p_{kj} \le p_{\max} x_{kj}, \forall k \in K, j \in J, \tag{5}$$

$$p_t = \sum_{k\in K}\sum_{j\in J} \delta_{kjt} p_{kj}, \forall t \in T, \tag{6}$$

$$\sum_{k\in K} x_{kj} \le n, \forall j \in J, \tag{7}$$

$$p_{\text{peak}} \ge p_t \forall t \in T, \tag{8}$$

$$x_{kj} \in \{0,1\}, q_{kj} \ge 0, p_{kj} \ge 0, \forall k \in K, j \in J. \tag{9}$$

Let K denote the set of daily charging events at the bus depot. Let J denote the set of charger occupancy sessions. This study divides a day into 96 charger occupancy sessions, so each charger occupancy session lasts for 15 min. Let T denote the minute set of a day. Let λ_{peak} represent the peak charging power price. Let λ_j denote the grid electricity price in session j. The continuous variable p_{peak} represents the peak charging power at the bus depot on a single day. The continuous variable q_{kj} indicates the amount of charged electricity of charging event k in session j. The objective function (1) minimizes the daily bus charging cost at the bus depot.

Let δ_{kj} denote an indicator parameter: 1 if charging event k covers session j or a part of session j and otherwise 0. Let x_{kj} denote a binary variable: 1 if the bus is charged in session j for charging event k and otherwise 0. Constraint (2) ensures that a bus is not charged in session j for charging event k when charging event k does not cover session j or a part of session j. Let Q_k denote the amount of charged electricity for charging event k. Constraint (3) ensures that the amount of charged

electricity should be met for charging event k. Let Δt_{kj} denote the charging time in session j for charging event k. The continuous variable p_{kj} represents the charging power in session j for charging event k. Constraint (4) presents the relationship between q_{kj} and p_{kj}. Let $p_{\max}$ denote the maximum allowable charging power for chargers. Therefore, constraint (5) reveals that the charging power p_{kj} should not exceed the maximum allowable charging power for chargers.

Let δ_{kjt} denote an indicator parameter: 1 if the charging event k in session j includes time t and otherwise 0. The continuous variable p_t indicates the total charging power at time t at the bus depot and is calculated as constraint (6) shows. Let n denote the number of chargers deployed at the bus depot. Constraint (7) ensures that the number of occupied chargers does not exceed the number of chargers deployed at the bus depot. Constraint (8) shows the logical relationship between p_{peak} and p_t.

Estimation of solar PV output power

Given the available area for installing PV panels at each bus depot, we first determine the maximum number of PV panels that can be installed at each bus depot. Let the tilt angle of PV panels α equal the latitude of Beijing[47]. Let the azimuth of PV panels β be 0°. We use sun power E20-327 PV module[48] in this study, and the detail of the parameters of this module is provided in Supplementary Table 4. Let a denote the PV module area (including the reserved area between two adjacent modules). We assume that the total gap area among PV panels account for 20% of the total suitable area. The maximum number of PV panels $N_{\max}$ at a bus depot with suitable area A is calculated as

$$N_{\max} = \frac{0.8A}{\cos(\alpha)a}. \tag{10}$$

Let I denote the solar irradiance on the PV module. Let β_{sun} denote the solar azimuth. Let α_{sun} denote the solar altitude. We use DNI and DHI to denote the direct normal irradiance and diffuse horizontal irradiance, respectively. Then I can be estimated with α, β, α_{sun}, β_{sun}, DNI and DHI[48]. Let T_{a} denote the air temperature. Let T_{n} denote the nominal operating cell temperature of the PV module. Let λ denote power temperature coefficient of the PV module. Let p denote the nominal power of the PV module. Then we employ a module parameter-based estimating model[48] to calculate the PV module output power Q as

$$Q = \frac{pI}{1,000}\left\{1 - \lambda\left[T_{\text{a}} + \frac{I}{800}(T_{\text{n}} - 20) - 25\right]\right\}. \tag{11}$$

However, we need to modify Q by considering energy loss and the differences among different PV modules since Q is derived according to a specific empirical formula. In Beijing, the PV solar generation for an installed capacity of 1 MW stands at about 1.2 million kWh in the first year[49]. On the basis of the calculation result of equations (10) and (11), the annual average PV solar generation for an installed capacity of 1 MW is 1.69 million kWh. This discrepancy necessitates the introduction of a correction factor κ, set at 0.71. The PV module output power Q is corrected by multiplying 0.71.

Maximizing economic profits of solar PV

The LCOE is a common metric used to measure the cost of electricity produced by renewable energy sources under a certain technical level. It is calculated as the ratio of the total lifetime cost to the total electricity production over that lifetime[38]. For the FiT scenario, the solar PV electricity sales price is established as the sum of the desulfurized coal benchmark price and subsidy price. A reasonable subsidy price is set to ensure that the PV electricity sales price exceeds the LCOE in this study. We set the PV electricity sales price for the no FiT scenario to equal the desulfurized coal benchmark price. Consequently, if the LCOE exceeds the desulfurized coal benchmark price, the PV electricity sales price will be lower than the LCOE, indicating a subsidy-free situation. For the grid parity scenario, the LCOE equals the desulfurized coal benchmark price, implying that the PV electricity sales price equals the LCOE. Hence, we entirely use available rooftop areas for PV panel deployments at each bus depot under the FiT and grid parity scenarios. We present the following mixed integer programming model for each bus depot to optimize the area of PV panel deployment under the no FiT scenario.

$$\min \lambda_{\text{peak}} p_{\text{peak}} + C_{\text{PV}} y + \sum_{k\in K}\sum_{j\in J}\lambda_j q_{kj} - \sum_{t\in T}\left[\lambda_t u_t + \lambda'_t(d_t y - u_t)\right], \tag{12}$$

$$x_{kj} \le \delta_{kj}, \forall k \in K, j \in J, \tag{13}$$

$$\sum_{j\in J} q_{kj} = Q_k, \forall k \in K, \tag{14}$$

$$q_{kj} = \Delta t_{kj} p_{kj}, \forall k \in K, j \in J, \tag{15}$$

$$p_{kj} \le p_{\max} x_{kj}, \forall k \in K, j \in J, \tag{16}$$

$$p_t = \sum_{k\in K}\sum_{j\in J}\delta_{kjt} p_{kj}, \forall t \in T, \tag{17}$$

$$\sum_{k\in K} x_{kj} \le n, \forall j \in J, \tag{18}$$

$$u_t \le \min\{\Delta t p_t, d_t y\}, \forall t \in T, \tag{19}$$

$$p_{\text{peak}} \ge p_t - \frac{u_t}{\Delta t}, \forall t \in T, \tag{20}$$

$$x_{kj} \in \{0,1\}, p_{kj} \ge 0, \forall k \in K, j \in J, \tag{21}$$

$$0 \le y \le y_{\max}, \tag{22}$$

$$u_t \ge 0, \forall t \in T. \tag{23}$$

Let C_{PV} denote the average daily cost (upfront and operational) of the solar PV project in the unit deployment area. Let λ_t denote the grid electricity price at time t. Let λ'_t denote the solar PV electricity sales price at time t. Let d_t denote the solar PV electricity generation in the unit deployment area at time t. The continuous variable y represents the deployment area of PV panels. The continuous variable u_t represents the amount of solar PV electricity used for charging BEBs at time t. Objective function (12) minimizes the sum of daily net operational and investment costs at the bus depot integrated with solar PV. Let Δt equal 1/60 h. Constraint (19) ensures that the amount of solar PV electricity used for charging BEBs at time t does not exceed the lesser of the bus charging demand and the solar PV electricity supply. Let $y_{\max}$ denote the maximum allowable deployment area of solar PV at the bus depot. Constraint (22) limits the range of solar PV deployment area. Finally, we use the average of y^* over 12 months to represent the optimal area of PV panel deployment.

In this study, we set a lifetime of 25 years for solar PV[50]. We also introduce a PV module ageing rate of 0.5% per year (ref. 51). Given the PV panel deployment area, we can continue to run the models (12)–(23) with varying d_t to optimize the daily PV use for different months and years.

Maximizing economic profits of solar PV and energy storage

We assume that the lifetime of the energy storage is 10 years (and assumed to be replaced after 10 years to match the PV system's lifetime).

Let the annual capacity degradation rate of the energy storage battery be 2.5%. We develop the following mixed integer programming model for each bus depot to optimize energy storage capacity and the PV panel deployment area jointly.

$$\min \lambda_{\text{peak}} p_{\text{peak}} + C_{\text{PV}} y + \sum_{k\in K}\sum_{j\in J} \lambda_j q_{kj} + \sum_{t\in T} \lambda_t g_{t,\text{grid,in}} - \sum_{t\in T} \left[\lambda_t (u_t + \eta_{\text{storage}} g_{t,\text{out}}) + \lambda'_t (d_t y - u_t - g_{t,\text{pv,in}})\right] + C_{\text{storage}} \bar{E}, \quad (24)$$

$$x_{kj} \le \delta_{kj}, \forall k \in K, j \in J, \quad (25)$$

$$\sum_{j\in J} q_{kj} = Q_k, \forall k \in K, \quad (26)$$

$$q_{kj} = \Delta t_{kj} p_{kj}, \forall k \in K, j \in J, \quad (27)$$

$$p_{kj} \le p_{\max} x_{kj}, \forall k \in K, j \in J, \quad (28)$$

$$p_t = \sum_{k\in K}\sum_{j\in J} \delta_{kjt} p_{kj}, \forall t \in T, \quad (29)$$

$$\sum_{k\in K} x_{kj} \le n, \forall j \in J, \quad (30)$$

$$p_{\text{peak}} \ge p_t - \frac{u_t}{\Delta t} - \frac{\eta_{\text{storage}} g_{t,\text{out}}}{\Delta t} + \frac{g_{t,\text{grid,in}}}{\Delta t}, \forall t \in T, \quad (31)$$

$$E_t = E_{t-1} + \eta_{\text{storage}} g_{t,\text{grid,in}} + \eta_{\text{storage}} g_{t,\text{pv,in}} - g_{t,\text{out}}, \forall t \in T, \quad (32)$$

$$0.2\bar{E} \le E_t \le \bar{E}, \forall t \in T, \quad (33)$$

$$E_0 = E_{1,440} = \bar{E}, \quad (34)$$

$$u_t + g_{t,\text{pv,in}} \le d_t y, \forall t \in T, \quad (35)$$

$$g_{t,\text{pv,in}} + g_{t,\text{grid,in}} \le \omega \Delta t, \forall t \in T, \quad (36)$$

$$\eta_{\text{storage}} g_{t,\text{out}} + u_t \le \Delta t p_t, \forall t \in T, \quad (37)$$

$$g_{t,\text{out}} \le \kappa \Delta t, \forall t \in T, \quad (38)$$

$$g_{t,\text{pv,in}} + g_{t,\text{grid,in}} \le B z_{t,\text{in}}, \forall t \in T, \quad (39)$$

$$g_{t,\text{out}} \le B z_{t,\text{out}}, \forall t \in T, \quad (40)$$

$$z_{t,\text{in}} + z_{t,\text{out}} \le 1, \forall t \in T, \quad (41)$$

$$x_{kj} \in \{0,1\}, p_{kj} \ge 0, \forall k \in K, j \in J, \quad (42)$$

$$0 \le y \le y_{\max}, \quad (43)$$

$$u_t \ge 0, \forall t \in T, \quad (44)$$

$$g_{t,\text{pv,in}}, g_{t,\text{grid,in}}, g_{t,\text{out}} \ge 0, \forall t \in T, \quad (45)$$

$$z_{t,\text{in}}, z_{t,\text{out}} \in \{0,1\}, \forall t \in T. \quad (46)$$

Let η_{storage} denote the energy storage efficiency and C_{storage} denote the average daily cost (upfront and operational) of energy storage in the unit capacity. The continuous variable $\bar{E}$ represents the energy storage capacity at the bus depot. The continuous variable $g_{t,\text{grid,in}}$ indicates the amount of grid electricity for charging energy storage at time t. The continuous variable $g_{t,\text{pv,in}}$ represents the amount of solar PV electricity for charging energy storage at time t. The continuous variable $g_{t,\text{out}}$ denotes the amount of energy storage electricity for charging BEBs at time t. Objective function (24) minimizes the sum of the daily net operational and investment costs at the bus depot integrated with solar PV and energy storage. Constraints (32)–(34) jointly limit the SoC of energy storage. Constraint (35) indicates that the amount of solar PV electricity used does not exceed the solar PV yield. Let ω denote the maximum allowable charging or discharging power of energy storage. We assume that this value can be derived from the C rate of energy storage. Therefore, constraint (36) restricts the amount of charged electricity for energy storage. Constraint (37) indicates that the charging supply does not exceed the charging demand. Constraint (38) restricts the amount of discharged electricity by energy storage. Let B denote a sufficiently large number. Let $z_{t,\text{in}}$ denote a binary variable: 1 if the energy storage is charged at time t and otherwise 0. Let $z_{t,\text{out}}$ denote a binary variable: 1 if the energy storage discharges at time t and otherwise 0. Hence, constraints (39)–(41) jointly ensure that the energy storage cannot receive and discharge simultaneously.

We use the average of y^* and $\bar{E}^*$ over 12 months to represent the optimal area of PV panel deployment and energy storage capacity, respectively. With the two decision variables fixed, we can continue to apply the models (24)–(46) to optimize the daily solar PV and energy storage use for varying months and years.

Impact assessment on grid loads

We calculate the net grid loads of BEB charging at time t at the bus depot in a month in a year as follows.

$$p_{\text{net,PV},t} = p_t - \frac{u_t}{\Delta t}, \quad (47)$$

$$p_{\text{net,PES},t} = p_t - \frac{u_t}{\Delta t} - \frac{\eta_{\text{storage}} g_{t,\text{out}}}{\Delta t} + \frac{g_{t,\text{grid,in}}}{\Delta t}. \quad (48)$$

where $p_{\text{net,pv}}$ and $p_{\text{net,PES}}$ represent the net grid loads of BEB charging at time t at the bus depot with integrating PV and PES, respectively.

Economic evaluation

Without adopting solar PV, the total charging cost of the public transport system during the lifetime of solar PV associated with a bus depot, CC_{total}, is calculated as

$$\text{CC}_{\text{total}} = \sum_{r\in R} \frac{\sum_{m\in M} \left[D_m \lambda_t \sum_{t\in T} \Delta t p_{r,m,t} + \lambda_{\text{peak},m} p_{\text{peak},r,m}\right]}{(1 + \text{discount rate})^r}. \quad (49)$$

Let R denote the set of solar PV lifetime years. Let M denote the set of months in a year. Let $p_{r,m,t}$ indicate the total charging power at time t in month m in year r. Let D_m denote the number of days in month m. Let $\lambda_{\text{peak},m}$ denote the fixed monthly price of peak charging power in month m. Let $p_{\text{peak},m}$ denote the peak charging power in month m.

The saving of BEB charging costs due to integrating PV, $S_{\text{c,PV}}$, is calculated as follows.

$$S_{\text{c,PV}} = \text{CC}_{\text{total}} - \sum_{r\in R} \frac{\sum_{m\in M} \left[D_m \lambda_t \sum_{t\in T} \Delta t p_{\text{net,PV},r,m,t} + \lambda_{\text{peak},m} p_{\text{net,PV,peak},r,m}\right]}{(1 + \text{discount rate})^r}. \quad (50)$$

where $p_{\text{net,PV},r,m,t}$ indicates the net grid load of BEB charging at time t in month m in year r with integrating PV and $p_{\text{net,PV,peak},r,m}$ represents the net peak charging power in month m in year r with integrating PV.

Let $R_{f,PV}$ denote the total lifetime feed-in revenue with integrating PV, which can be obtained by calculating the amount of PV electricity sold each year over the lifetime.

$$R_{f,PV} = \sum_{r\in R} \frac{\sum_{m\in M} D_m \sum_{t\in T} \lambda_t^{'}[(1-0.5\%\times r)\times d_t y - u_{r,m,t}]}{(1+\text{discount rate})^r}. \quad (51)$$

where $u_{r,m,t}$ represents the amount of solar PV electricity used for charging BEBs at time t in month m in year r.

The saving of BEB charging costs due to integrating PES, $S_{c,PES}$, is calculated as follows.

$$S_{c,PES} = CC_{total} - \sum_{r\in R} \frac{\sum_{m\in M}[D_m \lambda_t \sum_{t\in T} \Delta t p_{net,PES,r,m,t} + \lambda_{peak,m} p_{net,PES,peak,r,m}]}{(1+\text{discount rate})^r}. \quad (52)$$

where $p_{net,PES,r,m,t}$ indicates the net grid load of BEB charging at time t in month m in year r with integrating PES and $p_{net,PES,peak,r,m}$ represents the net peak charging power in month m in year r with integrating PES.

Let $R_{f,PES}$ denote the total lifetime feed-in revenue with integrating PES. $R_{f,PES}$ can be obtained as follows.

$$R_{f,PES} = \sum_{r\in R} \frac{\sum_{m\in M} D_m \sum_{t\in T} \lambda_t^{'}[(1-0.5\%\times r)\times d_t y - u_{r,m,t} - g_{r,m,t,pv,in}]}{(1+\text{discount rate})^r}. \quad (53)$$

where $g_{r,m,t,pv,in}$ represents the amount of solar PV electricity for charging energy storage at time t in month m in year r.

Let $C_{grid,PES}$ denote the total cost of grid electricity purchase for charging energy storage.

$$C_{grid,PES} = \sum_{r\in R} \frac{\sum_{m\in M} D_m \sum_{t\in T} \lambda_t g_{r,m,t,grid,in}}{(1+\text{discount rate})^r}. \quad (54)$$

where $g_{r,m,t,grid,in}$ represents the amount of grid electricity purchase for charging energy storage at time t in month m in year r.

The total cost (upfront and operational) of solar PV (C_{PV}) can be determined by the product of the PV installed capacity and the unit PV installed capacity cost. The upfront and operational energy storage cost is obtained by the product of the energy storage capacity and the unit energy storage capacity cost. Note that the salvage value of energy storage is considered when the energy storage system retires. Therefore, the total energy storage cost (C_{PES}) is defined as the difference between the upfront and operational cost and the salvage value. In this study, we assume that the resale price of energy storage equals 50% of the original cost for the unit energy storage capacity.

CO_2 emissions savings calculation

In ref. 13, the carbon emissions and electricity production of the global electricity industry in 2020, 2030, 2040 and 2050 are projected. We calculate the ratios of the carbon emissions to electricity production in 2020, 2030, 2040 and 2050. From 2021 to 2045, we calculate the average reductions in these calculated ratios between 2020 and 2030, between 2030 and 2040 and between 2040 and 2045, respectively. Therefore, we can extend the calculated ratios in every year of between 2021 to 2045. Finally, according to China's grid carbon emissions factor in 2021 (ref. 52), we extrapolate China's future carbon emissions factors to align with the trends of the extended ratios. Let E_{pv} denote the carbon emissions of solar PV during the solar PV lifetime. Let $E_{storage}$ denote the carbon emissions of energy storage during the solar PV lifetime. E_{pv} can be obtained by calculating the product of the solar PV production (kWh) and carbon emissions per solar PV production of 1 kWh (ref. 53). We obtain $E_{storage}$ by calculating the product of the energy storage capacity (kWh) and carbon emissions per energy storage capacity of 1 kWh (ref. 54). Consequently, we can obtain the total CO_2 savings during the solar PV lifetime according to the methodologies launched by Clean Development Mechanism[55].

$$EC_{pv} = -E_{pv} + \sum_{r\in R} \text{factor}_r \sum_{m\in M} D_m \sum_{t\in T} u_{r,m,t}, \quad (55)$$

$$EC_{pes} = -E_{pv} - E_{storage} + \sum_{r\in R} \text{factor}_r \sum_{m\in M} D_m \sum_{t\in T} (u_t + \eta_{storage} g_{r,m,t,out} - g_{r,m,t,grid,in}). \quad (56)$$

where EC_{pv} and EC_{pes} denote the total CO_2 savings during the solar PV lifetime with PV and PES at the bus depot, respectively. Let $g_{r,m,t,out}$ denote the amount of energy storage electricity for charging BEBs at time t in month m in year r. We use factor_r (as presented in Supplementary Table 7) to denote the estimated carbon emissions factors of the power industry of China in year r.

The marginal abatement costs of PV and PES are calculated as follows.

$$MAC_{PV} = \frac{C_{PV} - S_{c,PV} - R_{f,PV}}{EC_{pv}}, \quad (57)$$

$$MAC_{PES} = \frac{C_{PV} + C_{PES} + C_{grid,PES} - S_{c,PES} - R_{f,PES}}{EC_{pes}}. \quad (58)$$

where MAC_{PV} and MAC_{PES} represent the marginal abatement costs of PV and PES, respectively.

Data availability

The geolocation and rooftop area data of bus depots in Beijing are available from AMAP (Gaode Map) (https://www.amap.com/). The sampling data of historical energy consumption and charging profiles for battery electric buses in Beijing are available via an existing research article (https://www.pnas.org/doi/10.1073/pnas.2017318118) (ref. 41). The Beijing weekday load data for different months are available at https://www.ndrc.gov.cn/xxgk/zcfb/tz/201912/t20191230_1216857_ext.html. The projected global electricity generation and the corresponding carbon emissions from 2020 to 2050 are available at https://www.iea.org/reports/net-zero-by-2050. The two-part tariff of electricity price scheme for sizeable industrial electricity consumption in Beijing is available at https://www.beijing.gov.cn/zhengce/zhengcefagui/201905/W020190522525837842583.pdf. The datasets of air temperature, direct normal irradiance and diffuse horizontal irradiance are available from the China Meteorological Administration, but restrictions apply to the availability of these data, which were used under license for the current study and so are not publicly available. The data are, however, available from the authors upon reasonable request and with the permission of the China Meteorological Administration. The GPS trajectory data of 1,000 buses are available at https://github.com/Lejin99/GPS-data-of-1000-buses-in-Beijing. The source file for ref. 32 can be accessed via https://github.com/Lejin99/2022-Beijing-Public-Transport-Statistics-Report. The other datasets that support the findings of this study are available from the corresponding author upon reasonable request.

Code availability

The vehicle GPS trajectory data were processed using SQL Server and Python. The mixed integer linear programming models were solved using Gurobi. All the codes are available on request from the corresponding author.

References

1. Isik, M., Dodder, R. & Kaplan, P. O. Transportation emissions scenarios for New York City under different carbon intensities of electricity and electric vehicle adoption rates. *Nat. Energy* **6**, 92–104 (2021).

2. Creutzig, F. et al. Transport: a roadblock to climate change mitigation? *Science* **350**, 911–912 (2015).
3. *Total Final Consumption (TFC) by Sector World 1990–2020* (IEA, 2022); https://www.iea.org/data-and-statistics/data-tools/energy-statistics-data-browser?country=WORLD&fuel=Energy%20consumption&indicator=CO2Industry
4. *CO_2 Emissions from Transport Rebounded in 2021, Returning to their Historical Growth Trend* (IEA, 2022); https://www.iea.org/energy-system/transport
5. *Transport: Sectoral Overview* (IEA, 2022); https://www.iea.org/reports/transport
6. *Cars and Vans* (IEA, 2023); https://www.iea.org/energy-system/transport/cars-and-vans
7. Milovanoff, A., Posen, I. D. & MacLean, H. L. Electrification of light-duty vehicle fleet alone will not meet mitigation targets. *Nat. Clim. Change* **10**, 1102–1107 (2020).
8. Schäfer, A. W. & Yeh, S. A holistic analysis of passenger travel energy and greenhouse gas intensities. *Nat. Sustain* **3**, 459–462 (2020).
9. Jiang, Y., Zhou, Z. & Liu, C. The impact of public transportation on carbon emissions: a panel quantile analysis based on Chinese provincial data. *Environ. Sci. Pollut. Res.* **26**, 4000–4012 (2019).
10. He, H. et al. China's battery electric vehicles lead the world: achievements in technology system architecture and technological breakthroughs. *Green Energy Intell. Transp.* **1**, 100020 (2022).
11. *How Did Shenzhen, China Build World's Largest Electric Bus Fleet?* (World Resources Institute, 2018); https://www.wri.org/insights/how-did-shenzhen-china-build-worlds-largest-electric-bus-fleet
12. *China Tackles Climate Change with Electric Buses* (Institute for Transportation and Development Policy, 2018); https://www.itdp.org/2018/09/11/electric-buses-china/
13. *Net Zero by 2050: A Roadmap for the Global Energy Sector* (IEA, 2021); https://www.iea.org/reports/net-zero-by-2050
14. Powell, S., Cezar, G. V., Min, L., Azevedo, I. M. L. & Rajagopal, R. Charging infrastructure access and operation to reduce the grid impacts of deep electric vehicle adoption. *Nat. Energy* **7**, 932–945 (2022).
15. Sun, C., Zhao, X., Qi, B., Xiao, W. & Zhang, H. Economic and environmental analysis of coupled PV-energy storage-charging station considering location and scale. *Appl. Energy* **328**, 119680 (2022).
16. Ren, H., Ma, Z., Fong, M. L. & Sun, Y. Optimal deployment of distributed rooftop photovoltaic systems and batteries for achieving net-zero energy of electric bus transportation in high-density cities. *Appl. Energy* **319**, 119274 (2022).
17. Chen, X. et al. Impacts of fleet types and charging modes for electric vehicles on emissions under different penetrations of wind power. *Nat. Energy* **3**, 413–421 (2018).
18. Yap, K. Y., Chin, H. H. & Klemeš, J. J. Solar energy-powered battery electric vehicle charging stations: current development and future prospect review. *Renewable Sustain. Energy Rev.* **169**, 112862 (2022).
19. *The Xinqiao Electric Vehicle Charging Station has been Put Into Use, Becoming the First 'Solar PV Storage and Charging' Integrated Electric Vehicle Charging Station in Shanghai* (SOHU, 2017); https://www.sohu.com/a/196116998_391469
20. *The First Photovoltaic Bus Charging Station in Fujian Province is Put into Operation* (Quanzhou People Government, 2019); http://www.quanzhou.gov.cn/zfb/xxgk/zfxxgkzl/qzdt/xsqdt/201910/t20191024_1931604.htm
21. *The First Charging Station Integrated with Solar PV and Energy Storage in Hangzhou* (Baijiahao Baidu, 2019); https://baijiahao.baidu.com/s?id=1648902669522352818&wfr=spider&for=pc
22. *The First Charging Station Integrated with Solar PV and Energy Storage has been Put into Operation at Xi'an Xianyang International Airport* (Shanxi People Government, 2019); http://www.shaanxi.gov.cn/sy/sp/sxxwlb/201911/t20191103_1589392.html
23. *The First Charging Station Integrated with Solar PV and Energy Storage has been Completed in Chongqing* (Baijiahao Baidu, 2022); https://baijiahao.baidu.com/s?id=1748536321637598723&wfr=spider&for=pc
24. Ouammi, A. Peak load reduction with a solar PV-based smart microgrid and vehicle-to-building (V2B) concept. *Sustain. Energy Technol. Assess.* **44**, 101027 (2021).
25. Zhuang, P. & Liang, H. Stochastic energy management of electric bus charging stations with renewable energy integration and B2G capabilities. *IEEE Trans. Sustain. Energy* **12**, 1206–1216 (2021).
26. Luo, Y. et al. Coordinative planning of public transport electrification, RESs and energy networks for decarbonization of urban multi-energy systems: a government-market dual-driven framework. *IEEE Trans. Sustain. Energy* **15**, 538–555 (2024).
27. Ren, H., Ma, Z., Fai Norman Tse, C. & Sun, Y. Optimal control of solar-powered electric bus networks with improved renewable energy on-site consumption and reduced grid dependence. *Appl. Energy* **323**, 119643 (2022).
28. Mominul Islam, S. M., Salema, A. A., Saleheen, M. Z. & Lim, J. M. The influence of shifting the electric bus charging routine on the techno-economic performance of a solar-powered bus depot. *Energy* **239**, 122316 (2022).
29. Zaneti, L. A. L., Arias, N. B., de Almeida, M. C. & Rider, M. J. Sustainable charging schedule of electric buses in a university campus: a rolling horizon approach. *Renewable Sustain. Energy Rev.* **161**, 112276 (2022).
30. Liu, X., Liu, X. C., Xie, C. & Ma, X. Impacts of photovoltaic and energy storage system adoption on public transport: a simulation-based optimization approach. *Renewable Sustain. Energy Rev.* **181**, 113319 (2023).
31. *Statistical Data of Beijing Public Transport;* http://www.bjbus.com/home/fun_statistics.php?uSec=00000186&uSub=00000186
32. *Beijing Transport Development Annual Report* (Beijing Public Transport, 2022); https://www.bjtrc.org.cn/List/index/cid/7.html
33. *The First Innovative Three-Dimensional Charging Station in China* (Longruisanyou, 2023); https://www.longruisanyou.com/chargingStation/index/
34. Ding, T. et al. Review of optimization methods for energy hub planning, operation, trading, and control. *IEEE Trans. Sustain. Energy* **13**, 1802–1818 (2022).
35. Geidl, M. et al. Energy hubs for the future. *IEEE Power Energy Mag.* **5**, 4–30 (2007).
36. *Notice on the Perfection of Price Policy for the Power Generated by Solar PV, No. 1549* (National Development and Reform Commission, 2011); https://www.ndrc.gov.cn/xxgk/zcfb/tz/201108/t20110801_964803.html
37. Zhang, A. H., Sirin, S. M., Fan, C. & Bu, M. An analysis of the factors driving utility-scale solar PV investments in China: how effective was the feed-in tariff policy? *Energy Policy* **167**, 113044 (2022).
38. Yan, J., Yang, Y., Campana, P. E. & He, J. City-level analysis of subsidy-free solar photovoltaic electricity price, profits and grid parity in China. *Nat. Energy* **4**, 709–717 (2019).
39. *Clean Vehicles Directive* (European Commission, 2019); https://transport.ec.europa.eu/transport-themes/clean-transport/clean-and-energy-efficient-vehicles/clean-vehicles-directive_en
40. *Notice of the Beijing Municipal Development and Reform Commission on Adjusting the Electricity Price* (People's Government of Beijing Municipality, 2019); https://www.beijing.gov.cn/zhengce/zhengcefagui/201905/W020190522525837842583.pdf

41. Zhao, Y., Wang, Z., Shen, Z. J. M. & Sun, F. Assessment of battery utilization and energy consumption in the large-scale development of urban electric vehicles. *Proc. Natl Acad. Sci. USA* **118**, e2017318118 (2021).
42. Wang, Z. et al. *Annual Report on the Big Data of New Energy Vehicle in China* (China Machine Press, 2023).
43. Gallet, M., Massier, T. & Hamacher, T. Estimation of the energy demand of electric buses based on real-world data for large-scale public transport networks. *Appl. Energy* **230**, 344–356 (2018).
44. *Electric Bus Model Display* (Foton Auv, 2023); https://auv.foton.com.cn/webback/car/carList?jump=4
45. Lam, L. & Bauer, P. Practical capacity fading model for Li-Ion battery cells in electric vehicles. *IEEE Trans. Power Electron.* **28**, 5910–5918 (2013).
46. *Cycle Life Requirements and Test Methods for Traction Battery of Electric Vehicle* (National Technical Committee of Auto Standardization, 2015); http://www.catarc.org.cn/index.html
47. Rowlands, I. H., Kemery, B. P. & Beausoleil-Morrison, I. Optimal solar-PV tilt angle and azimuth: an Ontario (Canada) case-study. *Energy Policy* **39**, 1397–1409 (2011).
48. Chandra Mouli, G. R., Bauer, P. & Zeman, M. System design for a solar powered electric vehicle charging station for workplaces. *Appl. Energy* **168**, 434–443 (2016).
49. *The Photovoltaic Coverage Rate on the Roofs of Newly Built Public Institution Buildings, Parks, and Factories in Beijing Shall not be Less than 50%* (BJ News, 2023); https://www.bjnews.com.cn/detail/167999180314871.html
50. Wang, Y. et al. Accelerating the energy transition towards photovoltaic and wind in China. *Nature* **619**, 761–767 (2023).
51. Georgitsioti, T., Pearsall, N., Forbes, I. & Pillai, G. A combined model for PV system lifetime energy prediction and annual energy assessment. *Sol. Energy* **183**, 738–744 (2019).
52. *Notice on Key Work Related to the Management of Greenhouse Gas Emission Reports for Enterprises in 2022* (Ministry of Ecology and Environment of the People's Republic of China, 2022); https://www.mee.gov.cn/xxgk2018/xxgk/xxgk06/202203/t20220315_971468.html
53. IPCC *Climate Change 2014: Mitigation of Climate Change* (eds Edenhofer, O. et al) (Cambridge Univ. Press, 2014); https://www.ipcc.ch/report/ar5/wg3/
54. Li, P., Xia, X. & Guo, J. A review of the life cycle carbon footprint of electric vehicle batteries. *Sep. Purif. Technol.* **296**, 121389 (2022).
55. *AMS-I.F.: Renewable Electricity Generation for Captive Use and Mini-Grid—Version 2.0* (Clean Development Mechanism, 2017); https://cdm.unfccc.int/methodologies/DB/9V3T8W0N5PMCJH4YVEA04YYFTVHP3Q

Acknowledgements

X.M. acknowledges funding from Beijing Nova Program (20230484432) and National Key R&D Program of China (2023YFB2604600). S.Y. and P.P. gratefully acknowledge support by the EU STORM project funded from the European Union's Horizon 2020 programme (grant agreement number 101006700). P.P. has been supported within the project HOLA (FKZ 03EMF0404A) funded by the German Federal Ministry for Digital and Transport. S.Y. acknowledges funding from the European Union's Horizon 2020 research and innovation programme under grant agreement number 821124 and Mistra Carbon Exit.

Author contributions

X.L. and X.M. conceived and designed the study in consultation with P.P., S.Y. and X.C.L. X.L. collected the data, implemented the model and created the visualizations. Z.L. processed the bus GPS data. P.P., S.Y., X.L. and X.M. wrote the original manuscript with contributions from all co-authors.

Competing interests

The authors declare no competing interests.

Additional information

Supplementary information The online version contains supplementary material available at https://doi.org/10.1038/s41560-024-01580-0.

Correspondence and requests for materials should be addressed to Xiaolei Ma.

Peer review information *Nature Energy* thanks Kelvin Say and the other, anonymous, reviewer(s) for their contribution to the peer review of this work.